C. R. Mecanique 347 (2019) 365–375

Contents lists available at ScienceDirect

Comptes Rendus Mecanique

www.sciencedirect.com

Patterns and dynamics: homage to Pierre Coullet / *Formes et dynamique : hommage à Pierre Coullet*

Self-similar vortex reconnection

Reconnection des vortex auto-similaire

Sergio Rica [a,b,c,*]

[a] *Facultad de Ingeniería y Ciencias, Universidad Adolfo Ibáñez, Santiago, Chile*
[b] *Physics Center, Universidad Adolfo Ibáñez, Santiago, Chile*
[c] *LadHyX, CNRS, École polytechnique, Palaiseau, France*

ARTICLE INFO

Article history:
Received 1 September 2018
Accepted 23 November 2018
Available online 11 April 2019

Keywords:
Vortex reconnection
Vortex filaments
Gross–Pitaevskii equation
Self-similar solutions

Mots-clés :
Reconnection de vortex
Filaments de vorticité
Équation de Gross–Pitaevskii
Solutions auto-similaires

ABSTRACT

As shown by Crow in 1970, the evolution of two almost parallel vortex filaments with opposite circulation exhibits a long-wave instability. Ultimately, the symmetric mode increases its amplitude reconnecting both filaments and ending into the formation of an almost periodic structure of vortex rings. This is a universal process, which appears in a wide range of scales: from the vortex trails behind an airplane to a microscopic scale of superfluids and Bose–Einstein condensates. In this paper, I will focus on the vortex reconnection for the latter case by employing Gross–Pitaevskii theory. Essentially, I focus on the well-known laws of interaction and motion of vortex filaments. By means of numerical simulations, as well as theoretically, I show that a self-similar finite-time dynamics manifests near the reconnection time. A self-similar profile is selected showing excellent agreement with numerical simulations.

RÉSUMÉ

Comme le montre Crow en 1970, l'évolution de deux filaments de vortex presque parallèles à circulation opposée présente une instabilité à grand longueur d'onde. Le mode symétrique augmente d'amplitude en reconnectant les deux filaments et se termine par la formation d'une structure presque périodique d'anneaux de vortex. Il s'agit d'un processus universel qui apparaît à différentes échelles : des allées de vortex derrière un avion à l'échelle microscopique des superfluides et des condensats de Bose–Einstein. Dans cet article, je me concentre sur la reconnection de vortex pour le dernier cas en utilisant la théorie de Gross–Pitaevskii. Je me concentre essentiellement sur les lois bien connues de l'interaction et du mouvement des filaments de vortex. À l'aide de simulations numériques ainsi que théoriquement, je montre qu'une dynamique en temps fini auto-similaire se manifeste près du temps de reconnection. Un profil auto-similaire est sélectionné, montrant un excellent accord avec les simulations numériques.

* Correspondence to: Facultad de Ingeniería y Ciencias, Universidad Adolfo Ibáñez, Santiago, Chile.
E-mail address: sergio.rica@uai.cl.

https://doi.org/10.1016/j.crme.2019.03.011
1631-0721/

1. Introduction

In 1992, Lim and Nickels, from Melbourne, performed an extraordinary experiment on the instability and reconnection of opposite circulation vortex rings aligned in a perfect head-on scattering [1–3]. The experiment, done in water, consisted of the head-on collision of two equal circular vortices. According to the self-induction law, the vortex rings move ahead, however, as the vortex rings approach, because of mutual interaction, the ring radius increases, resulting in a simultaneous expansion of both vortex rings.[1] Further, as the radius increases, an instability develops, being amplified with an almost periodic modulation. Eventually, the amplitudes of deformation are large enough, leading to vortex reconnection and to radial momentum transfer by the emission of small vortex rings. Interestingly, the inverse configuration, namely a number of small vortex rings converging to a point resulting into the emergence of two vortex rings moving in opposite directions, was recently observed in experiments on air [4,5].

As already recognized by Lim and Nickels, when the vortex radius becomes sufficiently large, the dominant interaction comes from the opposite vortex ring, hence the situation may be regarded as that of two almost parallel vortex filaments with opposite circulation, a problem studied by Crow, from the Boeing company, in 1970 [6]. Crow's instability concerns the development of a long-wave instability for the separation distance of almost antiparallel drifting vortex filaments in an inviscid fluid. Crow shows that ultimately the symmetric mode increases its amplitude, reconnecting both filaments and ending into the formation of an almost periodic structure of vortex rings.

In a different context, vortex reconnections have regained interest in the last ten years in the context of helium-2 superfluid, since the experiment of Bewley, Lathrop and collaborators [7,8]. Because superfluid helium is essentially inviscid below 1 K and vortex circulation is quantized, helium-2 appears to be an excellent candidate to test Lim and Nickels and Crow instabilities. However, being extremely complicated in comparison with ordinary fluids, the two fluid behavior of helium-2 does not help from a theoretical point of view. Nevertheless, the $T = 0$ K behavior of a Bose–Einstein condensate (BEC) shares perfectly the desired phenomenology of vortex dynamics, hence instability and vortex reconnection. Bose–Einstein condensates are perfectly understood in terms of the Gross–Pitaevskii equation for the macroscopic wave function ψ, which is, finally, related to the one-particle density matrix of the system [9,10]. The Gross–Pitaevskii equation is a nonlinear Schrödinger equation (NLS), which is also a time-dependent nonlinear partial differential equation but simpler than Euler or Navier–Stokes equations for fluids (rephrasing AC Newell: "BEC, at $T = 0$, are easier to understand than they are to drink").

The nonlinear Schrödinger equation reads [11]:

$$\mathrm{i}\frac{\partial}{\partial t}\psi = -\frac{1}{2}\Delta\psi + g|\psi|^2\psi \tag{1}$$

here $\Delta = \nabla^2$ is the usual Laplacian in 3D, we used dimensionless variables and all parameters are set to one, being $g = \pm 1$ a sign variable that distinguishes the defocusing case ($g = 1$) from the focusing case ($g = -1$). From now on, we focus our attention to the former case. NLS shares many desired features in an infinite domain:

(i) it possesses a number of invariances: phase invariance, translational and rotational invariance, a dilatation invariance, Galilean invariance, and it is time reversible;
(ii) it preserves the number of particles, the energy and both linear and angular momentum;
(iii) from a mathematical point of view, it is a Hamiltonian dynamics;
(iv) weak and long-wave perturbations correspond to non-dispersive acoustic modes;
(v) equation (1) admits topological defects as exact solutions that represent quantized vortices. These are non-singular solutions for ψ. Moreover, the vortex core parameter naturally appears to be the balance among the non-linear and linear terms [12]. This distance, called the healing length (ξ_0), is of the order of one in the dimensionless units used in (1). The existence of this intrinsic length makes a crucial difference regarding the motion of vortex filaments in ordinary fluids, in which case a core dynamics is expected [13–15]. A proof of the above is the recently observed vorticity dynamics on head-on collisions of vortex rings [3].

Because of the simplicity of NLS, and due to these mathematical properties, it appears to be an attractive model for Bose–Einstein condensates and it has been extensively studied during the last 50 years. In particular, the Crow instability was studied by Berloff and Roberts [16], and it was recognized that the number of small vortex rings created depends on the initial separation distance of the two traveling vortices, however no link was identified with the problem of vortex reconnection. In superfluids, vortex reconnection has been studied long ago in the frame of the Biot–Savart filament dynamics [17,18] and as well as for the nonlinear Schrödinger equation [19].

The self-similar character of vortex reconnections was recognized by Pumir and Siggia [13,14] since the mid 1980s in connection with ordinary fluids and, in the context of superfluids, it was recently highlighted [8,20–22] (see Ref. [21] and references therein for more details).

In what it follows, Section 2 shows numerical simulations of the Crow instability in the frame of NLS for the cases of two anti-parallel vortex filaments and two head-on vortex rings collision. Next, Section 3 introduces the vortex interaction

[1] Something easily observed as a smoke vortex ring collides into a wall (the wall creates an image vortex in the opposite direction).

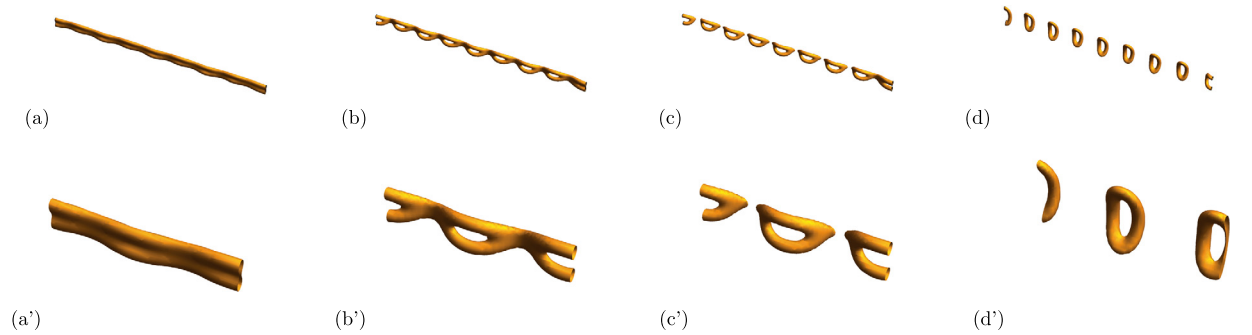

Fig. 1. Snapshots of the anatomy of vortex reconnection by the Crow instability mechanism. The initial separation distance was 3 units of length. (a) A modulational instability starts to develop; in (b) is shown the fore-vortex-reconnection instant; (c) shows the after-vortex-reconnection instant, and (d) shows the further evolution of 8 drifting vortex rings. The time sequence is (a) $t = 30$, (b) $t = 38$, (c) $t = 40$, and (d) $t = 50$. The second row plots a zoom of the same time sequence. The three dimensional surface plot shows the iso-surface $|\psi|^2 = 0.4$ and the simulations evolved into a cubic lattice of $N = 256^3$ with a mesh size $dx = 0.5$ (length units) and time step $dt = 0.01$.

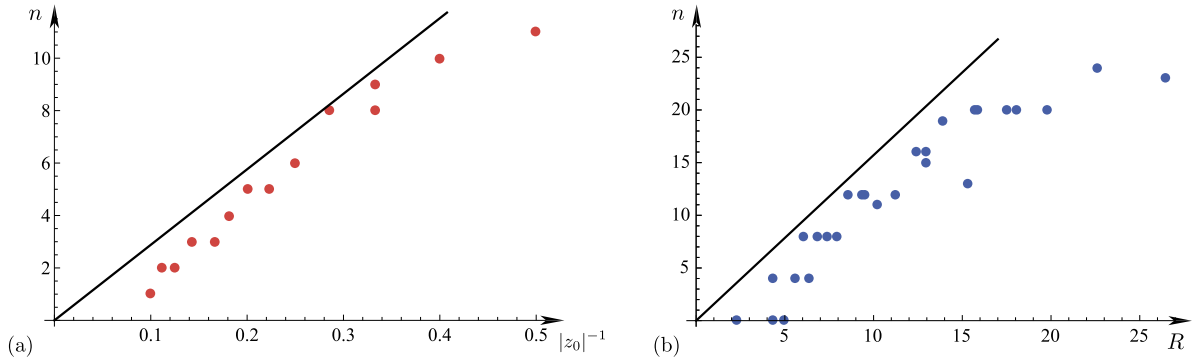

Fig. 2. (a) Number of vortex rings as a function of the inverse of the initial distance z_0. As a visual guide the line represents: $n = \frac{\sqrt{2}L}{2\pi}\frac{1}{|z_0|}$ (see Section 2 for the theoretical justification). The initial separation distances are such that $|z_0| \in [2, 10]$. The upper bound, 10, being the largest separation distance that can be allowed by the modulational instability because one gets just a single loop at the end. (b) Number of vortex rings after the collision of two circular vortex rings colliding head-on. The line represents $n = \frac{\pi R}{2}$. All simulations were done into a cubic lattice of $N = 256^3$ with a mesh size $dx = 0.5$ and a time step $dt = 0.01$.

of two parallel filaments in the frame of an incompressible and inviscid fluid. Section 4 provides evidence of self-similar vortex reconnection. Section 5 discuss the non-local effects of vortex interactions and its consequences. Finally, Section 6 concludes the current work.

2. Crow instability in the frame of the nonlinear Schrödinger equation

2.1. Antiparallel vortex instability

The time-dependent Gross–Pitaevskii equation (1) is solved with an initial condition $\psi_0(x, y, z)$, which vanishes at two parallel lines aligned within the z-axis and a separation distance $|z_0|$ (for the notations, see Section 3.2 below), which is a parameter that can be varied as desired. The resulting, initial condition corresponds to two topological defects. Figs. 1a–a' show two parallel vortex filaments with a slight sinusoidal displacement (similar results are obtained with a noisy perturbation of the position of the vortex filaments). As time passes, the vortex pair drifts as expected; moreover, the vortex distance perturbation is amplified, reconnecting the two vortex lines (Figs. 1b–b' & c–c'), ending with an array of traveling vortex rings (Figs. 1d–d').

By varying the separation distance, $|z_0|$, of the initial vortex pair, one notices that the number of vortices nucleated after the reconnection process scales as $n \sim 1/|z_0|$, see Fig. 2a.

2.2. Circular vortex ring instability

Next, we start with an initial condition consisting of two circular vortex rings with the same radii aligned along the z-axis, and placed head-on to ensure a frontal collision. Because of self-induction, the vortex rings drift one against the other colliding at the mid-point. As they come together, the self-induction becomes weaker than the interaction between the two rings, so they drift into the orthogonal plane increasing its radius and becoming unstable by a mechanism similar to that of the Crow's instability. Ultimately, a number of small vortex rings are ejected (Fig. 3).

(a) (b) (c) (d)

Fig. 3. Snapshots for the instability of two colliding vortex rings. The initial condition consists of two vortex rings of the same radii: $R = 12.4 \pm 0.5$ units. (a) The two vortex rings drifting head-on, (b) vortex rings approaching with the subsequent stretching of the circular filament, (c) the modulational instability and (d) vortex reconnection into 16 smaller vortex rings drifting into the orthogonal plane. The time sequence is (a) $t = 160$, (b) $t = 220$, (c) $t = 250$ and (d) $t = 270$. The three dimensional surface plot shows the iso-surface of $|\psi|^2 = 0.5$. The simulations evolved into a cubic lattice of $N = 256^3$ with a mesh size $dx = 0.5$ and a time step $dt = 0.01$.

3. Dynamics of two parallel vortex filaments

3.1. The effective vortex interactions

Because of the existence of an intrinsic length, the non-linear Schrödinger model makes it possible to reach a well-defined asymptotic limit in which the vortex filaments are faraway separated. Under this assumption, the full wave function is described by its phase and by the motion of vortex tubes of fixed size ξ_0. Briefly, $\psi \approx e^{i\Theta}$ with $\nabla^2\Theta = 0$, plus boundary conditions imposed by the vortex filaments. The resulting dynamics is driven by the Biot–Savart law of vortex interactions [12].

Consider first the dynamics of two rectilinear parallel vortex filaments, the first with circulation Γ_1 and located at $\boldsymbol{r}_1(t) = (x_1(t), y_1(t), s)$, and a second vortex with Γ_2 and located at $\boldsymbol{r}_2(t) = (x_2(t), y_2(t), s)$. The length parametrization s describes the fact that the vortices are rectilinear and parallel. The dynamics for the location of the vortices are the well known Hemholtz equations[2] [23]

$$\frac{d}{dt} z_1(t) = i\Gamma_2 \frac{(z_1(t) - z_2(t))}{|z_1(t) - z_2(t)|^2} \quad \text{and} \quad \frac{d}{dt} z_2(t) = -i\Gamma_1 \frac{(z_1(t) - z_2(t))}{|z_1(t) - z_2(t)|^2} \tag{2}$$

which are written, using complex notations, as: $z_1(t) = x_1(t) + i y_1(t)$ and $z_2(t) = x_2(t) + i y_2(t)$.

For the case of almost parallel vortex filaments, the position becomes a curve $\boldsymbol{r}_1(s,t) = (x_1(s,t), y_1(s,t), s)$, and similarly for $\boldsymbol{r}_2(s,t)$. The net interaction over the filament 1 has two contributions: the Biot–Savart flow created by the second vortex filament, which leads to an interaction like (2), and the self-interaction of filament 1 [12,17]. If the vortex filament curvature is small (that is, if the terms below (3) satisfy $|\partial_{ss} z_1(s,t)| \,\&\, |\partial_{ss} z_2(s,t)| \ll 1/\xi_0$) the Biot–Savart self-interaction may be approximated by the local induction approximation (LIA). The two contributions then read

$$\begin{aligned} \frac{\partial}{\partial t} z_1(s,t) &= i\Gamma_1 \frac{\partial^2}{\partial s^2} z_1(s,t) + i\Gamma_2 \frac{(z_1(s,t) - z_2(s,t))}{|z_1(s,t) - z_2(s,t)|^2} \\ \frac{\partial}{\partial t} z_2(s,t) &= i\Gamma_2 \frac{\partial^2}{\partial s^2} z_2(s,t) - i\Gamma_1 \frac{(z_1(s,t) - z_2(s,t))}{|z_1(s,t) - z_2(s,t)|^2} \end{aligned} \tag{3}$$

We emphasize that the second terms in (3) are valid if both filaments are asymptotically straight lines parallel to the $\hat{\boldsymbol{z}}$ axis. We postpone to Section 5 of the paper some considerations on the effects of non-locality of vortex interactions.

Defining $Z(s,t) = z_1(s,t) + z_2(s,t)$, $z(s,t) = z_1(s,t) - z_2(s,t)$ and setting $\Gamma_2 = -\Gamma_1 = -\Gamma$, for the case of two counter rotating almost parallel filaments, one gets the coupled nonlinear partial differential equations:

$$\frac{\partial}{\partial t} Z(s,t) = i\Gamma \frac{\partial^2 z}{\partial s^2} - 2i\Gamma \frac{z}{|z|^2} \tag{4}$$

$$\frac{\partial}{\partial t} z(s,t) = i\Gamma \frac{\partial^2 Z}{\partial s^2} \tag{5}$$

due to Klein, Majda, and Damodaran [24]. Similarly to Eqs. (2) and (3), equations (4) and (5) are derived from an action principle given by the Lagrangian density

$$\mathcal{L} = i\left(z(s,t)\partial_t Z^*(s,t) - z^*(s,t)\partial_t Z(s,t)\right) + \Gamma\left(|\partial_s z(s,t)|^2 + |\partial_s Z(s,t)|^2\right) + 2\Gamma \log|z(s,t)|^2 \tag{6}$$

Symmetry arguments provide the following conserved quantities through Noether's theorem [24]:

[2] Through the paper we use a different notation for the circulation, namely $\oint \boldsymbol{v} \cdot d\boldsymbol{\ell} = 2\pi\Gamma$ instead of Γ.

(i) the Hamiltonian $H = \Gamma \int \left(|\partial_s z(s,t)|^2 + |\partial_s Z(s,t)|^2 + 2\log|z(s,t)|^2\right) \mathrm{d}s$,
(ii) the mean of vorticity: $\Omega = \Gamma \int z(s,t)\mathrm{d}s$,
(iii) the angular momentum: $L = \int \left(Z(s,t)z^*(s,t) + Z^*(s,t)z(s,t)\right) \mathrm{d}s$,
(iv) and, $W = \frac{\mathrm{i}}{2} \int \left(Z(s,t)\partial_s z^*(s,t) - Z^*(s,t)\partial_s z(s,t) + z(s,t)\partial_s Z^*(s,t) - z^*(s,t)\partial_s Z(s,t)\right) \mathrm{d}s$.

Equations (4) and (5) for the vortex dynamics are the basic object that we study in the current paper.

3.2. Linear stability analysis

Consider the stability of uniform parallel counter propagating vortices. For the uniform case, no dependence on s is allowed, so that the uniform solution reads $z = z_0$, which represents the separation distance between both vortex filaments. Conversely, $Z_0(t) = -2\mathrm{i}\Gamma \frac{z_0}{|z_0|^2} t$ represents the uniform motion of the vortex pair. Perturbing this uniform solution as

$$Z(s,t) = -2\mathrm{i}\Gamma \frac{z_0}{|z_0|^2} t + \delta Z(s,t), \quad \text{and} \quad z(s,t) = z_0 + \delta z(s,t) \tag{7}$$

and linearizing the vortex dynamics (4)–(5), we get

$$\frac{\partial}{\partial t}\delta Z(s,t) = \mathrm{i}\Gamma \frac{\partial^2 \delta z}{\partial s^2} + 2\mathrm{i}\Gamma \frac{\delta \bar{z}}{z_0^2}, \quad \text{and} \quad \frac{\partial}{\partial t}\delta z(s,t) = \mathrm{i}\Gamma \frac{\partial^2 \delta Z}{\partial s^2}$$

Seeking perturbations of the form $\delta Z(s,t) \sim \mathrm{e}^{\mathrm{i}(ks-\omega t)}$, $\delta z(s,t) \sim \mathrm{e}^{\mathrm{i}(ks-\omega t)}$ and $\delta \bar{z}(s,t) \sim \mathrm{e}^{\mathrm{i}(ks-\omega t)}$, the linear problem provides a linear dispersion relation:

$$\omega_k^2 = \frac{\Gamma^2 k^2}{|z_0|^2}\left(|z_0|^2 k^2 \pm 2\right) \tag{8}$$

Among the four branches, two of them (the plus sign) correspond to Kelvin waves, while the other (the minus sign) may become unstable for $k|z_0| < \sqrt{2}$; this long-wave instability creates an exponential growth of the long-wave modes. The nonlinear regime of this instability ends with the formation of vortex rings of size of the order of the mean separation distance, $|z_0|$. More precisely, in a periodic system of size L, the wave numbers are quantized as $k_n = \frac{2\pi}{L} n$, therefore the unstable wave numbers are $\frac{2\pi}{L} n|z_0| < \sqrt{2}$, thus the selected number of unstable modes becomes $\frac{n}{L} < \frac{\sqrt{2}}{2\pi} \frac{1}{|z_0|}$. This relation is plotted, together with the numerical data, in Fig. 2a.

4. Self-similar vortex reconnection

4.1. Direct numerical simulations of (4) and (5)

Numerical simulations of the set of coupled partial differential Eqs. (4) and (5) show that the separation distance $z(s,t)$ vanishes in finite time. These equations are solved into a periodic domain $s \in [-L, L]$ with $L = 10$. For the numerical simulations, we consider a weakly initially modulated perturbation:

$$Z(s,0) = 0, \qquad z(s,0) = z_0\left(1 + \epsilon \sin\left(\frac{\pi}{L}s\right)\right) \tag{9}$$

This special class of initial condition preserves the initial values of $\mathrm{Im}\, z = 0$ and $\mathrm{Re}\, Z = 0$ [25]. However, other general initial conditions show similar self-similar behavior. For the sake of brevity, we focus the current paper on an initial condition of type (9). From the numerics, one observes that the vortex lines drift perpendicularly to the inter-vortex action line, as expected. However, because of the modulational instability, the small initial perturbations are amplified, creating a large deformation of the vortex lines and making the inter-vortex separation distance smaller; as a consequence, this portion drifts faster.

More quantitatively, supported by the simulations described in Fig. 4, we notice the following features:

(i) the appearing of a finite time singularity characterized by $z(s,t) \to 0$ as $t \to t_c$ and $Z(s,t) \to Z_0$, finite, as $t \to t_c$;
(ii) the minimum of $z(s,t)$ vanishes as $z(0,t) \sim (t_c - t)^{1/2}$; on the other hand, $Z(s,t)$ reaches a finite value: we can readily fit $Z(s,t) - Z_0 \sim (t_c - t)^{1/2}$;
(iii) a special kind of self-similar behavior is observed. Both z and Z scales as $(t_c - t)^{1/2}$, moreover, these functions must be re-scaled spatially with a self-similar coordinate $s(t_c - t)^{-1/2}$ (see Fig. 5).

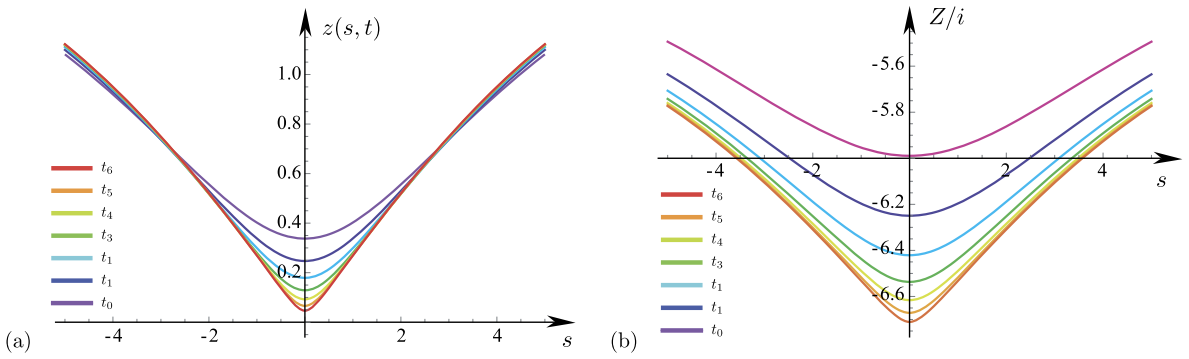

Fig. 4. Time evolution of the vortex filament variables $z(s,t)$ and $Z(s,t)$. (a) Plot of $z(s,t)$ for different time steps. (b) Plot of $Z(s,t)$ for same time steps as in (a). The simulations were done for $L=10$, an initial perturbation of the form (9) with $z_0=4$ and $\epsilon=0.1$ getting a finite time singularity at a time with $t_c\approx 44.756$. With initial condition (9), one has $t_c\approx 44.756$ and $Z_0\approx -27.223\mathrm{i}$. The time steps are $t_n=t_c-2^{1-n}$.

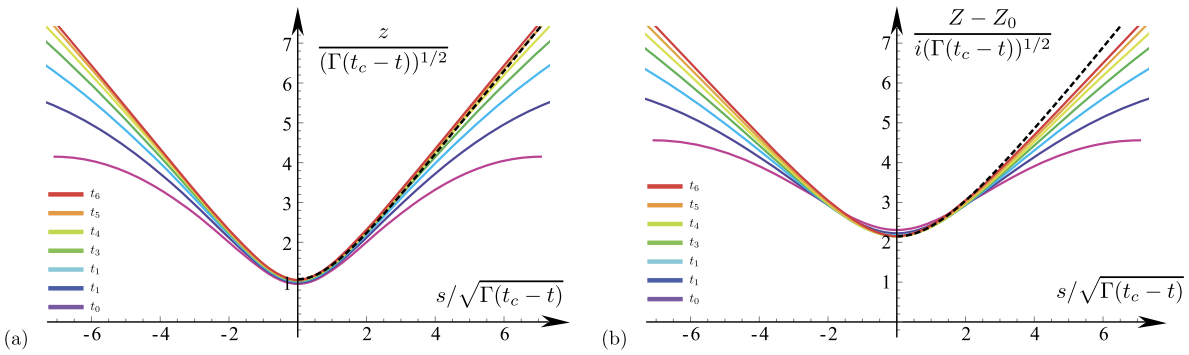

Fig. 5. Self-similar evolution of the re-scaled functions (10)–(11) as a function of the self-similar variable $\omega=s/\sqrt{\Gamma(t_c-t)}$. (a) Plots $z/\sqrt{\Gamma(t_c-t)}$) vs. ω and (b) $-\mathrm{i}(Z-Z_0)/\sqrt{\Gamma(t_c-t)}$) vs. ω. The segmented black line represents the solution to (13) and (14) with boundary conditions (15) and matching condition (22).

4.2. Self-similar solution for vortex reconnection

Accordingly with previous observations, we seek solutions of the form:

$$Z(s,t)=\mathrm{i}\left[Z_0+(\Gamma(t_c-t))^{1/2}\,\Phi\left(\frac{s}{\sqrt{\Gamma(t_c-t)}},-\log(t_c-t)\right)\right] \tag{10}$$

$$z(s,t)=(\Gamma(t_c-t))^{1/2}\,\zeta\left(\frac{s}{\sqrt{\Gamma(t_c-t)}},-\log(t_c-t)\right) \tag{11}$$

where $\Phi(\omega,\tau)$ and $\zeta(\omega,\tau)$ are two real functions of the re-scaled variables $\omega=s/\sqrt{\Gamma(t_c-t)}$ and $\tau=-\log(t_c-t)$.

The scaling $(t_c-t)^{1/2}$ has a long history. It was first recognized by Jean Leray in 1934 [26] (but with the fluid viscosity as a pre-factor), next, by Pumir and Siggia [13,14] in the frame of the Biot–Savart approximation for vortex filament motion in inviscid fluids. The current scaling, $\sqrt{\Gamma(t_c-t)}$, was explicitly found by Pomeau [27]. The same scaling arises in the case of superfluid helium [8], and finally measured accurately in direct numerical simulations of the NLS model [21].

Introducing the self-similar *Ansatz*, Eqs. (10) and (11), into the dynamical equations, one recovers the following set of partial differential equations for the self-similar variables:

$$\begin{aligned}\left(\frac{\partial}{\partial\tau}-\frac{1}{2}\left(1-\omega\partial_\omega\right)\right)\Phi(\omega,\tau)&=\left(\partial_{\omega\omega}\zeta(\omega,\tau)-\frac{2}{\zeta(\omega,\tau)}\right)\\ \left(\frac{\partial}{\partial\tau}-\frac{1}{2}\left(1-\omega\partial_\omega\right)\right)\zeta(\omega,\tau)&=-\partial_{\omega\omega}\Phi(\omega,\tau)\end{aligned} \tag{12}$$

As usual in this kind of problems, the desired solutions correspond to the stable fixed points of the nonlinear system [28]. That is, it is expected that time derivatives vanish in (12). These fixed points are solutions to the following set of ordinary differential equations:

$$-\frac{1}{2}\left(\Phi(\omega)-\omega\Phi'(\omega)\right)=\left(\zeta''(\omega)-\frac{2}{\zeta(\omega)}\right) \tag{13}$$

$$\frac{1}{2}\left(\zeta(\omega)-\omega\zeta'(\omega)\right)=\Phi''(\omega) \tag{14}$$

Equations (13) and (14) were first derived by Zakharov in 1988 [25]. Four boundary conditions are required to determine the solution. These may be derived from the conditions of regularity of the original variables (10)–(11). Following [28], one needs to impose:

$$\zeta'(0)=\Phi'(0)=0 \tag{15}$$

$$\zeta(\omega)\to\zeta_\infty^{\pm}\omega \quad \& \quad \Phi(\omega)\to\Phi_\infty^{\pm}\omega, \quad \omega\to\pm\infty \tag{16}$$

The constants $\zeta_\infty^{\pm}$ and $\Phi_\infty^{\pm}$ differ in the limits $\omega\to\pm\infty$. However, because of the even symmetry of the equations, and because of evidence coming from numerical simulations, one concludes that both slopes have the same absolute value: $|\zeta_\infty^{\pm}|=\zeta_\infty$ and $|\Phi_\infty^{\pm}|=\Phi_\infty$.

4.3. Inner asymptotic

The inner behavior of the solutions to (13) and (14) may be obtained from a regular asymptotic expansion of the form:

$$\zeta(\omega)=\sum_{n\geq 0}a_n\omega^n, \quad \text{and} \quad \Phi(\omega)=\sum_{n\geq 0}b_n\omega^n \tag{17}$$

Because of boundary conditions (15), $a_1=b_1=0$. Introducing the above asymptotic expansion into the nonlinear ODE system (13) and (14), one readily gets:

$$\begin{aligned} &a_2=\frac{1}{a_0}-\frac{b_0}{4}, \quad a_3=0, \quad a_4=\frac{(a_0^4+4a_0b_0-16)}{96a_0^3},\dots \\ &b_2=\frac{a_0}{4}, \quad b_3=0, \quad b_4=\frac{a_0b_0-4}{96a_0},\dots b_{2n+2}=-\frac{(2n-1)}{4(n+1)(2n+1)}a_{2n} \end{aligned} \tag{18}$$

Notice that because $a_1=b_1=0$, all odd coefficients vanish. This asymptotic expansion could be pursued up to all orders, and all coefficients depend only on a_0 and b_0.

4.4. Outer asymptotic

For the outer asymptotic, one needs to fit boundary conditions (16); therefore, we try the following asymptotic expansion for the solutions to (13) and (14)

$$\zeta(\omega)=\omega\sum_{n\geq 0}c_n\omega^{-n}, \quad \text{and} \quad \Phi(\omega)=\omega\sum_{n\geq 0}d_n\omega^{-n} \tag{19}$$

Here we identify $c_0\equiv\zeta_\infty$ and $d_0\equiv\Phi_\infty$. Introducing these asymptotic expansions into equations (13) and (14), one obtains:

$$\begin{aligned} &c_1=c_2=c_3=0, \quad c_4=\frac{2}{c_0}, \quad c_5=c_6=c_7=0, \quad c_8=-\frac{10(1+6c_0^2)}{c_0^3}, \quad c_9=c_{10}=c_{11}=0,\dots \\ &d_1=0, \quad d_2=\frac{2}{c_0}, \quad d_3=d_4=d_5=0, \quad d_6=-\frac{4(1+6c_0^2)}{3c_0^3}, \quad d_7=d_8=d_9=0,\dots \end{aligned}$$

The outer asymptotic shows that, for a given couple of parameters (c_0,d_0), the solution exhibits the correct behavior. Notice that none of the coefficients do depend explicitly on d_0 since $\Phi(\omega)=K\omega$ is always a solution, hence one cannot fix K.

4.5. Selection mechanism

Numerical solutions to the set (13)–(14) with the boundary conditions (15) show that in practice a given pair (a_0,b_0) selects a unique solution with the good asymptotic behavior (16); hence it provides a unique pair (c_0,d_0). However, there is a subtle point: although all solutions have the right behavior as $\omega\to\infty$, the original four-dimensional system has a natural tendency to display an oscillatory behavior. Looking for a general far-field ($\omega\to\infty$) solution, one notices that the original system becomes a purely linear equation (since $\zeta(\omega)\to\infty$). Taking $A(\omega)=\zeta(\omega)+\mathrm{i}\Phi(\omega)$, one gets that the linear problem may be reduced to a complex Hermite equation:

$$A''(\omega)+\frac{\mathrm{i}}{2}\omega A'-\frac{\mathrm{i}}{2}A=0 \tag{20}$$

which has two independent solutions:

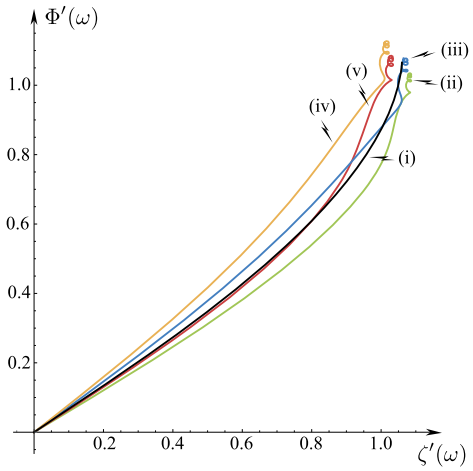

Fig. 6. Φ'–ζ' projection of the trajectories; five different trajectories are shown for parameters (a_0, b_0) taking the following values: (i) (1.071, 2.125); (ii) (1.044, 2.088); (iii) (1.106, 2.088); (iv) (1.044, 2.213); (v) (1.106, 2.213).

$$A_1(\omega) = 1 + \mathrm{i}\frac{\omega^2}{2\cdot 2!} + \frac{\omega^4}{2^2\cdot 4!} - \mathrm{i}3\frac{\omega^6}{2^3\cdot 6!} - \cdots = \mathrm{e}^{-\mathrm{i}\frac{\omega^2}{4}} + \mathrm{e}^{\mathrm{i}\frac{\pi}{4}}\omega f\left(\frac{\mathrm{e}^{\mathrm{i}\frac{\pi}{4}}}{2}\omega\right), \quad \& \quad A_2(\omega) = \omega \tag{21}$$

where $f(z) = \int_0^z \mathrm{e}^{-t^2}\mathrm{d}t$ is proportional to an error function. The total asymptotic solution is $A(\omega) = \alpha A_1(\omega) + \beta A_2(\omega)$, where α and β are complex numbers corresponding to four integration constants. Starting with (a_0, b_0), then the far-field behavior sets $\alpha = \alpha(a_0, b_0)$ and $\beta = \beta(a_0, b_0)$. Because the oscillatory behavior comes from $A_1(\omega)$, one concludes that by imposing the condition for the complex parameter $\alpha(a_0^*, b_0^*) = 0$, one gets two conditions for a_0^* and b_0^*. Moreover, the second complex parameter, $\beta(a_0^*, b_0^*) = c_0 + \mathrm{i}d_0$ provides the far-field asymptotic boundary conditions. In the numerics, one can see that this selection mechanism works for the values[3]:

$$a_0^* \approx 1.071 \quad \& \quad b_0^* \approx 2.125 \quad \Rightarrow \quad c_0^* \approx 1.0605 \quad \& \quad d_0^* \approx 1.0841 \tag{22}$$

Fig. 5 compares the self-similar functions with the self-similar envelope determined by direct numerical simulations of the original model, Eqs. (4) and (5). Fig. 6 shows the phase portrait in the ζ', Φ' projection plane of the suppression of the oscillatory mode for the parameter conditions (22).

Finally, the universal behavior of the closest relative distance between filaments is given by $z(s=0,t) = (\Gamma(t_c - t))^{1/2}\,\zeta\,(0) \equiv a_0^*(\Gamma(t_c - t))^{1/2}$. By comparing with the results of Ref. [21], before reconnection, namely their $\delta^-(t)$, one concludes that their A_- must be $A_- = \frac{a_0^*}{\sqrt{2\pi}} \approx 0.427$, in agreement with the numerical results of Ref. [21]. Moreover, the parameters c_0 and d_0 provide information for the reconnection angles. More precisely, the tangents of filament 1 behave, asymptotically, as $\hat{\boldsymbol{t}}_1^{\pm}$ as $s \to \pm\infty$, and the same occurs for filament 2. The respective opening angles between the filaments read:

(i) the opening angle of a single filament: $\cos\theta = -\hat{\boldsymbol{t}}_1^- \cdot \hat{\boldsymbol{t}}_1^+ = -\frac{4-c_0^2-d_0^2}{4+c_0^2+d_0^2}$, which is about $\theta \approx 105.66°$ for the values found in (22);

(ii) the opening angle between different filaments: $\cos\varphi = \hat{\boldsymbol{t}}_1^+ \cdot \hat{\boldsymbol{t}}_2^+ = \frac{4-c_0^2+d_0^2}{4+c_0^2+d_0^2}$; in this case, one gets $\varphi \approx 50°$.

The former opening angle is close to the numerical values found in Ref. [18], while the second angle appears to be twice the value given in the same reference.

5. Nonlocal effects on vortex dynamics

The self-similar scenario predicts a singular behavior of the filament curvature, yet the derivation of Eqs. (3) is valid for a vortex filament distance larger than the healing length, $|z(s,t)| \gg \xi_0$, for an almost straight pair of vortex filaments and for small filament curvature. When $t \to t_c$, then $|z(s,t)| \to 0$ and the self-similar curvature

[3] Essentially it is a two-parameter shooting method (treated in detail in Ref. [28]). A good visual method consists in plotting $\zeta'(\omega)$ vs. $\Phi'(\omega)$, because both functions start at the origin and they both reach a fixed point, (c_0, d_0), the oscillations been clearly observed in most of cases, excepting the selected ones.

$$\kappa(s,t) \sim \frac{1}{\sqrt{\Gamma(t_c-t)}} K\left(\frac{s}{\sqrt{\Gamma(t_c-t)}}\right) \tag{23}$$

blows up. In that situation, the vortex dynamics provided by Eqs. (3) must be revisited.

The filament dynamics comes from the Biot–Savart expression for the contributions of the velocity induced by the filament itself and the contributions of all the other filaments. For an almost straight filament considered in Eqs. (3), one gets the general filament dynamics:

$$\frac{\partial z_1(s)}{\partial t} = -\mathrm{i}\frac{\Gamma_1}{2}\int_{-\infty}^{\infty} \frac{z_1(s')-z_1(s)-(s'-s)z_1'(s')}{\left[(s-s')^2+|z_1(s)-z_1(s')|^2\right]^{3/2}}\mathrm{d}s' + \mathrm{i}\frac{\Gamma_2}{2}\int_{-\infty}^{\infty} \frac{z_1(s)-z_2(s')+(s'-s)z_2'(s')}{\left[(s-s')^2+|z_1(s)-z_2(s')|^2\right]^{3/2}}\mathrm{d}s' \tag{24}$$

and a similar equation for the second filament by exchanging 1 with 2. In what it follows, we analyze each term separately.

5.1. The self-interaction contribution

As it is well known, the first integral in (24) diverges logarithmically at $s=s'$. Introducing an arc-length cut-off, ℓ, one splits the self-interaction vortex dynamics into a couple of terms as:

$$\int_{-\infty}^{\infty} \frac{z_1(s')-z_1(s)-(s'-s)z_1'(s')}{\left[(s-s')^2+|z_1(s)-z_1(s')|^2\right]^{3/2}}\mathrm{d}s' = \log(\ell/\xi_0)\frac{\partial^2}{\partial s^2}z_1(s,t) + \int_{-\infty}^{\infty} \frac{z_1(s')-z_1(s)-(s'-s)z_1'(s')}{\left[(s-s')^2+|z_1(s)-z_1(s')|^2\right]^{3/2}}\mathrm{d}s'$$

Where we have defined a regularized integration

$$\int_{-\infty}^{\infty} f(s')\mathrm{d}s' \equiv \int_{-\infty}^{s-\ell} f(s')\mathrm{d}s' + \int_{s+\ell}^{\infty} f(s')\mathrm{d}s'$$

which removes the singular part of the Biot–Savart integral [17]. If the non-local integral term is discarded, one recovers the local induction term in (3) up to the logarithmic pre-factor $\frac{1}{2}\log(\ell/\xi_0)$, which can be absorbed with an adequate definition of the scale length s.

For the self-similar solutions of the form of the Ansatz (10) and (11), one recovers the same scaling equations (13) and (14) as before, but the nonlocal contribution modifies them. In particular, the ζ'' term in Eq. (13) changes as:

$$\zeta''(\omega) \to \zeta''(\omega) + \int_{-\infty}^{\omega-\ell/\sqrt{\Gamma(t_c-t)}} \frac{\zeta(\omega')-\zeta(\omega)-(\omega'-\omega)\zeta'(\omega')}{\left[(\omega-\omega')^2+\frac{1}{4}|\zeta(\omega)-\zeta(\omega')|^2+\frac{1}{4}|\Phi(\omega)-\Phi(\omega')|^2\right]^{3/2}}\mathrm{d}\omega' +$$
$$+ \int_{\omega+\ell/\sqrt{\Gamma(t_c-t)}}^{\infty} \frac{\zeta(\omega')-\zeta(\omega)-(\omega'-\omega)\zeta'(\omega')}{\left[(\omega-\omega')^2+\frac{1}{4}|\zeta(\omega)-\zeta(\omega')|^2+\frac{1}{4}|\Phi(\omega)-\Phi(\omega')|^2\right]^{3/2}}\mathrm{d}\omega'$$

and similarly for Φ'' in (14).

Because the integration limits in both integrals behave as $\omega' \to \omega \pm \ell/\sqrt{\Gamma(t_c-t)} \to \pm\infty$, when $t_c \to t$, one requires just the asymptotic behaviors of $\zeta(\omega') = c_0|\omega'|$ and $\Phi(\omega') = d_0|\omega'|$ in the integration. In that case, all integrals may be computed exactly for a fixed ω, leading to the expression:

$$\frac{8\Gamma(t_c-t)}{\ell^2\left(c_0^2+d_0^2+4\right)^{3/2}} \times (\zeta(\omega)-c_0\omega)$$

Therefore, the nonlocal contribution comes up to an order $\mathcal{O}(\Gamma(t_c-t))$, thus the nonlocal interaction may be discarded, when $t \to t_c$, in the self similar equations.

5.2. The filament interaction contribution

If the separation distance is almost constant in (24) in its asymptotic limit, one may safely replace:

$$\mathrm{i}\frac{\Gamma_2}{2}\int_{-\infty}^{\infty} \frac{z_1(s)-z_2(s')+(s'-s)z_2'(s')}{\left[(s-s')^2+|z_1(s)-z_2(s')|^2\right]^{3/2}}\mathrm{d}s' \to \mathrm{i}\Gamma_2\frac{(z_1(s,t)-z_2(s,t))}{|z_1(s,t)-z_2(s,t)|^2} \tag{25}$$

However, the far-field behavior (16) of self-similar functions appears to contradict this condition. Therefore, Eqs. (13) and (14) are modified as

$$-\frac{1}{2}\left(\Phi(\omega)-\omega\Phi'(\omega)\right)=\zeta''(\omega)-\frac{1}{2}\int_{-\infty}^{\infty}\frac{\zeta(\omega')+\zeta(\omega)-(\omega'-\omega)\zeta'(\omega')}{\left[(\omega-\omega')^2+\frac{1}{4}(\zeta(\omega)+\zeta(\omega'))^2+\frac{1}{4}(\Phi(\omega)-\Phi(\omega'))^2\right]^{3/2}}\mathrm{d}\omega'$$

$$\frac{1}{2}\left(\zeta(\omega)-\omega\zeta'(\omega)\right)=\Phi''(\omega)+\frac{1}{2}\int_{-\infty}^{\infty}\frac{\Phi(\omega')-\Phi(\omega)-(\omega'-\omega)\Phi'(\omega')}{\left[(\omega-\omega')^2+\frac{1}{4}(\zeta(\omega)+\zeta(\omega'))^2+\frac{1}{4}(\Phi(\omega)-\Phi(\omega'))^2\right]^{3/2}}\mathrm{d}\omega' \tag{26}$$

Hormoz and Brenner [15] have approximated the non-local effects of the second filament in the case of fluid dynamics, obtaining a non-universal vortex collision scenario. Although the problem is not precisely the same, because in ordinary fluids a core structure possesses a coupled dynamic, the selection mechanism for Eqs. (26) seems to be similar as discussed in Section 4.5. Naturally, the specific values of the parameters a_0^* and b_0^* (as well as c_0^* and d_0^*) must change. Indeed, in the far field, $\omega\to\pm\infty$, that is $\zeta(\omega)\to\infty$, both integrals also vanish. Therefore, the final far-field linear problem is ruled by the Hermite equation (20). As in Section 4.5, a condition for removing the oscillatory behavior must be imposed, leading probably to a universal solution. This program will be discussed in a future publication.

6. Discussion

It has been shown that the vortex dynamics of two almost anti-parallel vortex filaments display a finite-time singularity. By means of numerical simulations, as well as theoretically, we show that a self-similar finite-time dynamics manifests near the reconnection time. The filament distance vanishes in finite time and the vortex drift propagates up to a maximum value, producing a cusp. This self-similar profile satisfies an autonomous equation and a selection mechanism is introduced, showing excellent agreement with numerical simulations. However, some questions remain open.

(i) The uniqueness of the matching condition (22) and the stability of the self-similar profile. Usually these kinds of problems introduce a variety of solutions that satisfy the boundary conditions; however, not all of them are stable, therefore a stability analysis must complement the current analysis. Perhaps the existence of a variational principle for Eqs. (12), which reads[4]:

$$\mathcal{S}=\int \mathrm{e}^{-\frac{3}{2}\tau}\left[4\log\zeta+(\partial_\omega\zeta)^2+(\partial_\omega\Phi)^2+\zeta\left(2\partial_\tau\Phi+\omega\partial_\omega\Phi-\Phi\right)\right]\mathrm{d}\omega\,\mathrm{d}\tau$$

could shed light on the road to a plausible answer to this question.

(ii) An arbitrary initial condition (an arbitrary complex field for $z(s,t=0)$ and $Z(s,t=0)$ or for a non-symmetric initial perturbation with respect to the origin) requires a more careful study. Although $a_0\approx 1$ for all cases, it has been observed a slight discrepancy on the value of b_0, getting values greater than 3.

(iii) In the case of very close propagating vortices, it has been observed the nucleation of Jones-Roberts structures [29] instead of small vortex rings. The transverse fluctuations manifest themselves via a Kandomshev–Petshiavili instability that ultimately becomes a solitary wave [29].

(iv) Direct numerical simulations of the nonlinear Schrödinger equation, shown in Ref. [21], do not display a self-similar behavior for the filament curvature as in (23); however, in that case, the vortex reconnection dynamics is tracked near the collision point, namely the vortex separation distance is $|z(0,t)|\approx\xi_0$. Therefore, naturally, the approximations employed in the derivation of (4) and (5) are not valid near reconnection. In the same line, the post-reconnection scenario is not accessible in the frame of Eqs. (4) and (5); to do that, one should understand well the matching among the far-field dynamics [12]. Something that is still open in the author's opinion.

(v) *Note added in Proof.* Banica, Faou, and Miot [30] have shown, in the frame of Eqs. (3), the existence of a finite-time collision of counter-rotative vortex filaments described by non-differentiable self-similar solutions.

Acknowledgements

The author acknowledges inspiration by the lectures of G. Krstulovic, D. Proment and A. Pumir at the Foundation les Treilles, Tourtour, France, September 2017. He also thanks Isabelle Gallagher for providing Ref. [30], Marco Fontelos, Giorgio Krstulovic, and Davide Proment for critical reading of the manuscript, and Fernando Mora for his help. Financial support from the FONDECYT grant No. 1181382 and the "Dirección de Investigación" from "Universidad Adolfo Ibáñez" is acknowledged by the author. Finally, the author thanks the Gaspard Monge Visiting Professor Program of "École polytechnique" (France).

[4] This action is derived after the Lagrangian (6) together with the self-similar solutions (10) and (11), and the Jacobian coming from a change of variables from $(s,t)\to(\omega,\tau)$.

References

[1] T.T. Lim, T.B. Nickels, Instability and reconnection in the head-on collision of two vortex rings, Nature 357 (1992) 225–227.
[2] Smarter Every Day 195, Two vortex rings colliding in slow motion, https://www.youtube.com/watch?time_continue=19&v=EVbdbVhzcM4.
[3] R. McKeown, R. Ostilla-Mónico, A. Pumir, M. Brenner, S.M. Rubinstein, Emergence of small scales in vortex ring collisions, Phys. Rev. Fluids 3 (2018) 100509.
[4] R.H. Hernández, E. Monsalve, Experimental observation of the collision of three vortex rings, Fluid Dyn. Res. 47 (2015) 035513.
[5] R.H. Hernández, T. Reyes, Symmetrical collision of multiple vortex rings, Phys. Fluids 29 (2017) 103604.
[6] S.C. Crow, Stability theory for a pair of trailing vortices, AIAA J. 8 (1970) 2172–2179.
[7] G.P. Bewley, M.S. Paoletti, K.R. Sreenivasan, D.P. Lathrop, Characterization of reconnecting vortices in superfluid helium, Proc. Natl. Acad. Sci. USA 105 (2008) 13707.
[8] E. Fonda, D.P. Meichle, N.T. Ouellette, S. Hormoz, D.P. Lathrop, Direct observation of Kelvin waves excited by quantized vortex reconnection, Proc. Natl. Acad. Sci. USA 111 (2014) 4707.
[9] V.L. Ginzburg, L.D. Landau, On the theory of superconductivity, Zh. Eksp. Teor. Fiz. 20 (1950) 1064.
[10] O. Penrose, L. Onsager, Bose–Einstein condensation and liquid helium, Phys. Rev. 104 (1956) 576.
[11] L.P. Pitaevskii, Vortex lines in an imperfect Bose gas, Sov. Phys. JETP 13 (1961) 451;
E.P. Gross, Hydrodynamics of a superfluid condensate, J. Math. Phys. 4 (1963) 195–207.
[12] L.M. Pismen, Vortices in Nonlinear Fields: From Liquid Crystals to Superfluids, from Non-equilibrium Patterns to Cosmic Strings, Oxford University Press, 1999.
[13] E.D. Siggia, Collapse and amplification of a vortex filament, Phys. Fluids 28 (1985) 794.
[14] A. Pumir, E.D. Siggia, Vortex dynamics and the existence of solutions to the Navier–Stokes equations, Phys. Fluids 30 (1987) 1606.
[15] S. Hormoz, M.P. Brenner, Absence of singular stretching of interacting vortex filaments, J. Fluid Mech. 707 (2012) 191–204;
S. Hormoz, M.P. Brenner, Non-universal and non-singular asymptotics of interacting vortex filaments, Proc. IUTAM 7 (2013) 97–106.
[16] N.G. Berloff, P.H. Roberts, Motion in a Bose condensate: IX. Crow instability of antiparallel vortex pairs, J. Phys. A, Math. Gen. 34 (2001) 10057.
[17] K.W. Schwarz, Three-dimensional vortex dynamics in superfluid ^{4}He: line-line and line-boundary interactions, Phys. Rev. B 31 (1985) 5782.
[18] A.T.A.M. de Macle, R.G.K.M. Aarts, Route to vortex reconnection, Phys. Rev. Lett. 72 (1993) 482.
[19] J. Koplik, H. Levine, Vortex reconnection in superfluid helium, Phys. Rev. Lett. 71 (1993) 1375.
[20] L. Boué, D. Khomenko, V.S. L'vov, I. Procaccia, Analytic solution of the approach of quantum vortices towards reconnection, Phys. Rev. Lett. 111 (2013) 145302.
[21] A. Villois, D. Proment, G. Krstulovic, Universal and nonuniversal aspects of vortex reconnections in superfluids, Phys. Rev. Fluids 2 (2017) 044701.
[22] J. Reneuve, J. Salort, L. Chevillard, Structure, dynamics, and reconnection of vortices in a nonlocal model of superfluids, Phys. Rev. Fluids 3 (2018) 114602.
[23] H. Helmholtz, Über Integrale der hydrodynamischen Gleichungen, welche den Wirbelbewegungen entsprechen, J. Reine Angew. Math. 55 (1858) 25–55; Translation by P.G. Tait, On integrals of the hydrodynamical equations, which express vortex-motion, Philos. Mag. 33 (1867) 485–510.
[24] R. Klein, A.J. Majda, K. Damodaran, Simplified equations for the interaction of nearly parallel vortex filaments, J. Fluid Mech. 288 (1995) 201–248.
[25] V.E. Zakharov, Wave collapse, Usp. Fiz. Nauk 155 (1988) 529–533.
[26] J. Leray, Essai sur le mouvement d'un fluide visqueux emplissant l'espace, Acta Math. 63 (1934) 193–248.
[27] Y. Pomeau, Remarques sur l'instabilité d'un vortex axial, C. R. Acad. Sci. Paris, Ser. II 318 (1994) 865–870;
Y. Pomeau, Singularité dans l'évolution du fluide parfait, C. R. Acad. Sci. Paris, Ser. II 321 (1995) 407–411.
[28] J. Eggers, M.A. Fontelos, Singularities: Formation, Structure, and Propagation, Cambridge University Press, Cambridge, UK, 2015.
[29] C. Jones, P.H. Roberts, Motions in a Bose condensate. IV. Axisymmetric solitary waves, J. Phys. A, Math. Gen. 15 (1982) 2599–2619.
[30] V. Banica, E. Faou, E. Miot, Collision of almost parallel vortex filaments, Commun. Pure Appl. Math. 70 (2017) 378–405.